


Active droplet driven by a collective motion of enclosed microswimmersZhihan Huang,¹ Toshihiro Omori ^{1,*} and Takuji Ishikawa^{1,2}¹*Department of Finemechanics, Tohoku University, Aoba 6-6-01, Sendai, Miyagi, Japan*²*Department of Biomedical Engineering, Tohoku University, Aoba 6-6-01, Sendai, Miyagi, Japan*

(Received 9 April 2020; accepted 16 July 2020; published 6 August 2020)

Active fluids containing self-propelled particles are relevant for applications such as self-mixing, micropumping, and targeted drug delivery. With a confined boundary, active fluids can generate bulk flow inside the system, which has the potential to create self-propelled active matter. In this study, we propose that an active droplet is driven by a collective motion of enclosed microswimmers. We show that the droplet migrates via the flow field generated by the enclosed microswimmers; moreover, the locomotion direction depends on the swimming mode of these internal particles. The locomotion mechanism of the droplet can be well explained by interfacial velocity, and the locomotion velocity shows good agreement with the Lighthill-Blake theory. These findings are essential to understand the interplay between the motion of self-propelled particles and the bulk motion response of active matter.

DOI: [10.1103/PhysRevE.102.022603](https://doi.org/10.1103/PhysRevE.102.022603)**I. INTRODUCTION**

Active matter is capable of converting free energy into mechanical work and is relevant for many applications, such as self-mixing, micropumping, targeted drug delivery, biomimetic crawling, and self-healing [1–5]. In an active fluid containing self-propelled particles, active stress due to microswimmers is effectively exerted, resulting in interesting phenomena such as superfluidity, multiple mechanical equilibria, and hydrodynamic instability [6,7]. To take advantage of the anomalous properties of active fluids, we must first understand the interplay between the motions of individual self-propelled particles and the bulk motion of the active fluid. With a confined boundary, active suspensions, such as motile bacteria within circular boundaries [8], can generate stable flow patterns and coherent structures inside the boundary [9]. These swimmer-driven flows have the potential to create self-propelled active matter. For example, a solitary microswimmer confined within a droplet could break the symmetry and generate the net motion of the droplet. Reigh *et al.* [10] designed an active droplet with a confined single microswimmer. Force dipole on the swimmer’s body generated bulk flow within the droplet, and the droplet migrated in a specific direction depending on the sign of the force dipole. To design active matter powered by enclosed microswimmers, a collective motion of self-propelled particles should be utilized. However, many questions remain regarding the interplay between the collective motion of self-propelled particles and the bulk motion of the active fluid.

Swimming microorganisms are typical self-propelled particles, which have been well-studied in terms of fluid mechanics. One of the simplest mathematical models of a swimming microorganism is the Lighthill-Blake theory, in which a squirmer [11,12] propels itself by generating surface

squirring velocities. A squirmer can be classified as a “pusher-type,” a “puller-type,” or a “neutral-type” swimmer, based on the force dipole exerted on the body. The swimming modes govern the particle dynamics; for example, a pusher tends to escape from a free surface, whereas a puller may become entrapped at the interface [cf. Ref. [13] and Figs. 1(b) and 1(c)]. Motions of the squirmer near a free-surface or a solid wall are organized in Ref. [14]; if one is interested, please refer to it. Because different particle dynamics produce different flow structures, the bulk motion of active fluid is affected by the swimming mode. Additionally, the flow generated by a number of squirmers is sufficiently strong to advect and direct other swimmers [15], which leads to the bulk motion of an active fluid, such as that of self-organized coherent structures [16–18].

In this study, we propose an active droplet containing a number of squirmers. We show that the droplet can migrate via the flow generated by the collective motion of squirmers. The direction of locomotion is determined by the swimming mode of the internal particles. The locomotion mechanism of the droplet is well explained by the interfacial velocity, and the locomotion velocity shows good agreement with the Lighthill-Blake theory.

II. GOVERNING EQUATIONS AND NUMERICAL METHODS**A. Problem setting**

Consider N microswimmers confined within a droplet placed in an unbounded fluid with constant density ρ_{out} and viscosity μ , as shown in Fig. 1(a). Gravity acts in the negative z direction. The fluid inside the droplet has a smaller density ρ_{in} , but the same viscosity as its surrounding fluid μ (these conditions may be realized by a water droplet in a Fluorinert, for example). We assume that the droplet as a whole is neutrally buoyant. Thus, the relationship among the three

*omori@bfs1.mech.tohoku.ac.jp

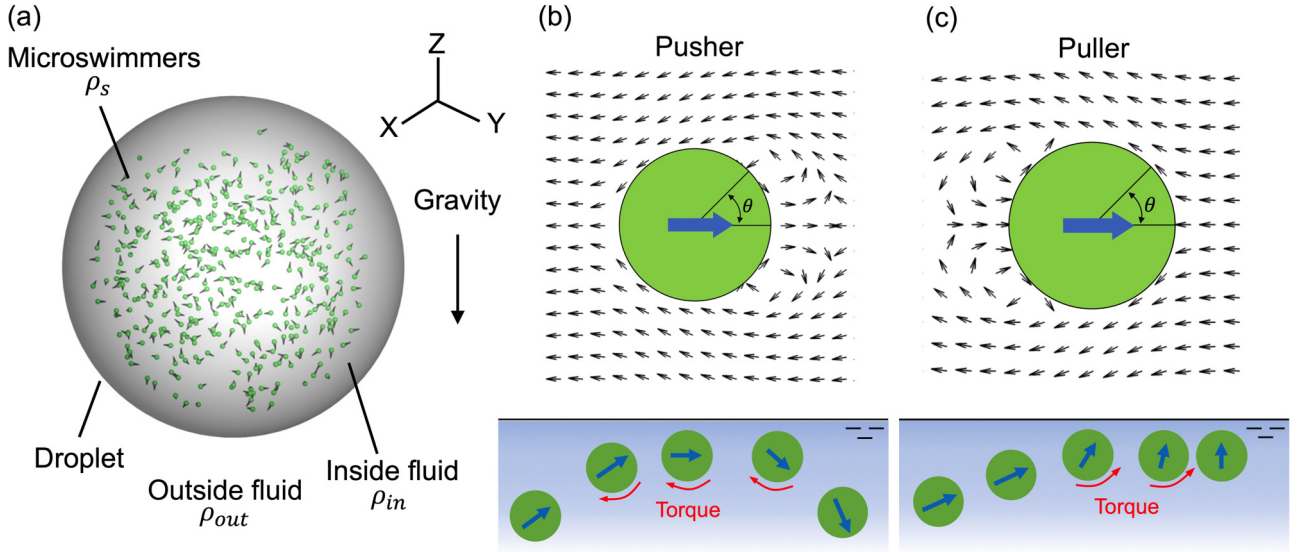


FIG. 1. Problem setting and squirmer types. (a) N microswimmers are confined within a droplet. The droplet as a whole is neutrally buoyant, and densities of microswimmers ρ_s , inside fluid ρ_{in} , and outside fluid ρ_{out} satisfy $\rho_s > \rho_{out} > \rho_{in}$. (b), (c) Flow created by a pusher-type squirmer and a puller-type squirmer with the swimmer's frame of reference. Due to hydrodynamic torque, the pusher tends to escape from a free surface, whereas the puller is entrapped at the interface [13].

densities is defined as $\rho_s > \rho_{out} > \rho_{in}$, where ρ_s is the density of the microswimmer. Due to its neutral buoyancy, the droplet will not move if the swimmers are inert. We also assume that the droplet is sufficiently small to describe the surrounding flow as viscous dominant, and the flow field is governed by the Stokes equation. The capillary number, defined as the ratio of viscous force to surface force $Ca = \mu U^d / \gamma$, is assumed to be appropriately small, where U^d is the locomotion velocity of the droplet and γ is the interfacial tension of the droplet surface. Hence, we neglect the deformation of the droplet. For the boundary condition, we assume continuous shear stress across the surface of the droplet: $\mathbf{q} \cdot \mathbf{t} = 0$, where $\mathbf{q} = [\sigma_{out} - \sigma_{in}] \cdot \mathbf{n}$ is the stress jump across the surface; σ is the stress tensor; the subscripts out and in indicate the outer surface and the inner surface, respectively; \mathbf{n} is the unit outward normal vector; and \mathbf{t} is the unit surface tangential vector. Furthermore, to satisfy the mass conservation and nondeformation of the droplet, we assume that surface flow in the normal direction is zero: $\mathbf{u}^{surf} \cdot \mathbf{n} = 0$, where \mathbf{u}^{surf} is the surface velocity relative to the center of the droplet.

B. Swimmer model: Squirmer

The microswimmer is modeled by a squirmer [11,12]. A squirmer is a spherical envelope model of ciliated microorganisms, and the velocity \mathbf{u}^s generated by the squirmering velocity is expressed as an infinite series of eigensolutions of the Stokes equation:

$$\begin{aligned} u_r^s(r, \theta) = & -U \cos \theta + A_0 \frac{a^2}{r^2} P_0 + \frac{2}{3} (A_1 + B_1) \frac{a^3}{r^3} P_1 \\ & + \sum_{n=2}^{\infty} \left\{ \left[\frac{1}{2} n \frac{a^n}{r^n} - \left(\frac{1}{2} n - 1 \right) \frac{a^{n+2}}{r^{n+2}} \right] A_n P_n \right. \\ & \left. + \left(\frac{a^{n+2}}{r^{n+2}} - \frac{a^n}{r^n} \right) B_n P_n \right\}, \end{aligned} \quad (1)$$

$$\begin{aligned} u_\theta^s(r, \theta) = & U \sin \theta + \frac{1}{3} (A_1 + B_1) \frac{a^3}{r^3} V_1 \\ & + \sum_{n=2}^{\infty} \left\{ \left[\frac{1}{2} n \frac{a^{n+2}}{r^{n+2}} - \left(\frac{1}{2} n - 1 \right) \frac{a^n}{r^n} \right] B_n V_n \right. \\ & \left. + \frac{1}{2} n \left(\frac{1}{2} n - 1 \right) \left(\frac{a^n}{r^n} - \frac{a^{n+2}}{r^{n+2}} \right) A_n V_n \right\}, \end{aligned} \quad (2)$$

where (r, θ) are spherical polar coordinates (cf. Fig. 1), a is the radius of the squirmer, A_n and B_n are coefficients of the series, U is the swimming speed of the squirmer, $P_n(\cos \theta)$ are Legendre polynomials, and

$$V_n = \frac{2 \sin \theta}{n(n+1)} P_n'. \quad (3)$$

Using a force-free condition so that the Stokeslet term must be zero, the swimming speed U corresponds to

$$U = \frac{1}{3} (2B_1 - A_1), \quad (4)$$

and the velocity at $r = a$ is given by

$$u_r^s(a, \theta) = \sum_{n=0}^{\infty} A_n P_n(\cos \theta), \quad u_\theta^s(a, \theta) = \sum_{n=1}^{\infty} B_n V_n(\cos \theta). \quad (5)$$

Assuming that the surface velocity is tangential, i.e., A_n is equal to zero for all n , the swimming velocity U is given by $U = 2B_1/3$, and the swimming mode β is given by the second mode: $\beta = B_2/B_1$. A squirmer with $\beta < 0$ is a pusher [Fig. 1(b)], a squirmer with $\beta > 0$ is a puller [Fig. 1(c)], and a squirmer with $\beta = 0$ is a neutral swimmer.

C. Motion of a microswimmer

We assume that the droplet as a whole is neutrally buoyant, and the relationship among the three densities is described by $\rho_s > \rho_{\text{out}} > \rho_{\text{in}}$. Then, the sedimentation force exerted on a microswimmer can be expressed as

$$\mathbf{F}^s = -\frac{4}{3}\pi(\rho_{\text{in}} - \rho_s)a^3\mathbf{g}, \quad (6)$$

and the flow field generated by sedimentation \mathbf{u}^s is given by

$$u_r^s(r, \phi) = -U^s \left(1 - \frac{3a}{2r} + \frac{a^3}{2r^3}\right) \cos \phi, \quad (7)$$

$$u_\phi^s(r, \phi) = U^s \left(1 - \frac{3a}{4r} + \frac{a^3}{4r^3}\right) \sin \phi, \quad (8)$$

where \mathbf{g} is the gravity, ϕ is the elevation angle relative to the gravity, and $U^s = |\mathbf{F}^s|/6\pi\mu a$.

In addition to sedimentation, we consider the bottom heaviness of the squirmer [19]. In some microorganisms, like *Volvox*, the centroid and center of mass are at different positions. Thus, an external torque is exerted on the body and propels the microorganism vertically upwards:

$$\mathbf{T}^{\text{bh}} = -\frac{4}{3}\pi\rho_s a^3 h \mathbf{g} \wedge \mathbf{e}, \quad (9)$$

where \mathbf{e} is the swimming direction of the squirmer and h is the distance between the centroid and the center of mass.

Locomotion of the i th squirmer can be described by a boundary integral equation using a velocity-additivity approximation [20,21]. The translational velocity of each squirmer is then described by summing self-swimming U , self-sedimentation U^s , squirmer-squirmer interactions according to Eqs. (1), (2), (7), (8), and (9), and squirmer-droplet interactions:

$$\frac{d\mathbf{x}_i}{dt} = U\mathbf{e}_i + \mathbf{U}^s + \sum_{j \neq i}^N \left(\mathbf{u}_{ij}^s + \mathbf{u}_{ij}^g + \frac{1}{8\pi\mu r_{ij}^3} \mathbf{T}_j^{\text{bh}} \wedge \mathbf{r}_{ij} \right) + \frac{1}{8\pi\mu} \int \mathbf{J}(\mathbf{x}_i, \mathbf{y}) \cdot \mathbf{q}(\mathbf{y}) dS_d(\mathbf{y}), \quad (10)$$

$$\frac{d\mathbf{e}_i}{dt} = \omega_i \wedge \mathbf{e}_i, \quad (11)$$

where S_d indicates the surface of the droplet and \mathbf{q} is the traction. The last term on the right-hand side of Eq. (10) indicates the flow generated by the viscous traction exerted on the droplet surface [22]. In other words, the Green's function $\mathbf{J} = \mathbf{I}/r + \mathbf{r} \otimes \mathbf{r}/r^3$ can associate the interface traction with the velocity. \mathbf{I} is the identity matrix, $r = |\mathbf{r}|$, and $\mathbf{r} = \mathbf{y} - \mathbf{x}_i$. Quantities with the subscript ij indicate the relative distance or flow between the i th and j th squirmers.

The angular velocity ω_i is defined in a similar manner, as follows:

$$\omega_i = \frac{\mathbf{T}_i^{\text{bh}}}{8\pi\mu a^3} + \nabla \wedge \left[\sum_{j \neq i}^N \left(\mathbf{u}_{ij}^s + \mathbf{u}_{ij}^g + \frac{1}{8\pi\mu r_{ij}^3} \mathbf{T}_j^{\text{bh}} \wedge \mathbf{r}_{ij} \right) + \frac{1}{8\pi\mu} \int \mathbf{J}(\mathbf{x}_i, \mathbf{y}) \cdot \mathbf{q}(\mathbf{y}) dS_d(\mathbf{y}) \right]. \quad (12)$$

The first term represents self-rotation due to bottom heaviness, and the latter represents rotation due to the squirmer-squirmer and the squirmer-droplet interactions.

III. MOTION OF A DROPLET

We assume that the droplet is sufficiently small to describe the surrounding flow as viscous dominant, and the flow field is governed by the Stokes equation. The flow field at arbitrary positions \mathbf{x} can be expressed by a boundary integral equation [22,23] in a similar manner to Eq. (10):

$$\mathbf{u}(\mathbf{x}) = \mathbf{u}^\infty(\mathbf{x}) - \frac{1}{8\pi\mu} \int \mathbf{J}(\mathbf{x}, \mathbf{y}) \cdot \mathbf{q}^d(\mathbf{y}) dS_d(\mathbf{y}) + \frac{1}{8\pi\mu} \int \mathbf{J}(\mathbf{x}, \mathbf{y}) \cdot (\rho_{\text{in}} - \rho_{\text{out}})\mathbf{g} dV'_d(\mathbf{y}), \quad (13)$$

where \mathbf{q}^d is the viscous traction, $V'_d = V_d - N \times 4\pi a^3/3$, and V_d is the volume of the droplet. The second term on the right-hand side of Eq. (13) indicates the flow due to the surface traction of the droplet, and the last term is the flow driven by the density gradient between the inner and outer fluids. \mathbf{u}^∞ is the flow generated by squirmers:

$$\mathbf{u}^\infty = \sum_i^N \left(\mathbf{u}_i^s + \mathbf{u}_i^g + \frac{1}{8\pi\mu r_i^3} \mathbf{T}_i^{\text{bh}} \wedge \mathbf{r} \right). \quad (14)$$

Assuming the droplet as a whole is neutrally buoyant, the force-free condition can be expressed as

$$\int \mathbf{q}^d dS_d = \mathbf{0}. \quad (15)$$

According to rigid motions of the droplet, the velocity at the surface of the droplet is given by

$$\mathbf{u}|_{r=a^d} = \mathbf{U}^d + \boldsymbol{\Omega}^d \wedge \hat{\mathbf{r}} + \mathbf{u}^{\text{surf}}, \quad (16)$$

where a^d is the droplet radius, \mathbf{u}^{surf} is the surface velocity relative to the droplet center, $\boldsymbol{\Omega}^d$ is the angular velocity of the droplet, $\hat{\mathbf{r}} = \mathbf{x} - \mathbf{x}_c$, and \mathbf{x}_c is the center of mass of the droplet. For the boundary condition, we assume $\mathbf{q}^d \cdot \mathbf{t} = 0$ and $\mathbf{u}^{\text{surf}} \cdot \mathbf{n} = 0$ at $\mathbf{x} \in S_d$, where \mathbf{t} and \mathbf{n} are tangential and normal unit vectors of the droplet surface, respectively. To meet the boundary conditions, the normal vector \mathbf{n} is multiplied by Eqs. (13), (15), and (16):

$$\begin{aligned} & \mathbf{u}(\mathbf{x}) \cdot \mathbf{n}(\mathbf{x}) \\ &= \mathbf{u}^\infty(\mathbf{x}) \cdot \mathbf{n}(\mathbf{x}) - \frac{1}{8\pi\mu} \int \mathbf{J}(\mathbf{x}, \mathbf{y}) \cdot \mathbf{q}^d(\mathbf{y}) \cdot \mathbf{n}(\mathbf{x}) dS_d(\mathbf{y}) \\ &+ \frac{1}{8\pi\mu} \int \mathbf{J}(\mathbf{x}, \mathbf{y}) \cdot (\rho_{\text{in}} - \rho_{\text{out}})\mathbf{g} \cdot \mathbf{n}(\mathbf{x}) dV'_d(\mathbf{y}), \end{aligned} \quad (17)$$

$$\int \mathbf{q}^d \cdot \mathbf{n} dS_d = 0, \quad (18)$$

and

$$\mathbf{u}|_{r=a^d} \cdot \mathbf{n} = \mathbf{U}^d \cdot \mathbf{n}. \quad (19)$$

We then solve above system with respect to the unknowns \mathbf{q}^d and \mathbf{U}^d .

IV. NUMERICAL METHOD

To calculate the values of the unknowns $\mathbf{q}^d (= q^d \mathbf{n})$ and \mathbf{U}^d , we use a boundary element method [21]. The droplet surface is discretized by \mathcal{N} triangle meshes, and the system

is discretized by a Gaussian numerical integration scheme:

$$\begin{bmatrix} \mathcal{A} & \mathcal{B} \\ \mathcal{C} & 0 \end{bmatrix} \begin{bmatrix} \mathbf{q}^d \\ \mathbf{U}^d \end{bmatrix} = \begin{bmatrix} \mathbf{u}^\infty \cdot \mathbf{n} \\ \mathbf{0} \end{bmatrix}. \quad (20)$$

Matrix components \mathcal{A} and \mathcal{B} are given by Eqs. (17) and (19), and \mathcal{C} is from Eq. (18), whose sizes are $\mathcal{N} \times \mathcal{N}$, $\mathcal{N} \times 3$, and $3 \times \mathcal{N}$, respectively. This dense matrix system is solved by a lower-upper factorization technique with a linear algebra library (CUSOLVER; NVIDIA). Once the viscous traction \mathbf{q}^d is obtained, the traction $\mathbf{q} = \mathbf{q}^d + \mathbf{q}^s$ is assigned to Eq. (10), where $\mathbf{q}^s(\mathbf{x}) = (\rho_{\text{in}} - \rho_{\text{out}})(\mathbf{g} \cdot \mathbf{x})\mathbf{n}(\mathbf{x})$. The positions of the squirmer and droplet are updated by a second-order Runge-Kutta method. The mesh number and the time step are set to $\mathcal{N} = 5$ and 120 and $\Delta t U/a = 5.0 \times 10^{-3}$, respectively, throughout this study (we confirmed mesh and time convergence using finer meshes and smaller time steps).

If the swimmers come too close to each other or the surface of the droplet, the solution is less accurate and numerical instabilities may arise. To avoid this, we added short-range repulsive forces. The short-range repulsive forces are assumed to act between two adjacent squirmers. The magnitudes of the forces acting on particles 1 and 2 are the same, and their directions are opposite. Such a pair of forces results in a force dipole, which can be modeled as a stresslet acting at the midpoint between two approaching squirmers. When two squirmers i and j are closer than $3a$, the repulsive stresslet is induced at the midpoint of two swimmers:

$$\mathbf{S}(\mathbf{x}_{ij}^m) = \mathbf{r}'_{ij} \otimes \mathbf{r}'_{ij} - \frac{1}{3}\mathbf{I}, \quad (21)$$

where $\mathbf{x}_{ij}^m = (\mathbf{x}_i + \mathbf{x}_j)/2$, $\mathbf{r}'_{ij} = \mathbf{r}_{ij}/|\mathbf{r}_{ij}|$, and $\mathbf{r}_{ij} = \mathbf{x}_j - \mathbf{x}_i$. We preliminarily confirmed that the distance $3a$ is sufficiently large to accurately describe the pairwise interaction using the velocity additivity method by comparing it to a boundary element method [24]. Then, the velocity generated by the stresslet is added to Eqs. (10) and (12):

$$\mathbf{u}^{\text{rep}} = c\mathbf{K} : \mathbf{S}, \quad (22)$$

where $\mathbf{K} = 3\mathbf{r} \otimes \mathbf{r} \otimes \mathbf{r}/r^5 - \mathbf{I}/r^3$ is the propagator for the stresslet. The constant c is set to 0.6π to prevent two swimmers having contact with each other.

When the squirmer approaches the surface of the droplet, within a distance of $0.01a$, lubrication torque is applied to the squirmer under the assumption that the interface is flat. The lubrication torque was calculated beforehand by a boundary element method using the image system of a flat free surface [13], and it acts to alter the swimming direction depending on the swimming mode β .

Here, we introduce a nondimensional parameter Gr , which represents the ratio between the gravitational and viscous forces acting on the microswimmers; $\text{Gr} = (\rho_s - \rho_{\text{in}})ga^2/\mu U$. The sedimentation velocity U^s is then expressed as $U^s/U = 2\text{Gr}/9$. The total neutral buoyancy condition is expressed as $N \times \frac{4\pi a^3}{3}\text{Gr} = \int \text{Gr}' dV'_d$, where N is the number of squirmers, V'_d is the effective volume of the droplet, and $\text{Gr}' = (\rho_{\text{out}} - \rho_{\text{in}})ga^2/\mu U$. The gravitational effects are cross-linked with Gr and the volume fraction through \mathbf{u}_{ij}^s in Eqs. (10) and (12). We then take Gr and the volume fraction as parameters, in addition to studying a number of swimming modes β .

V. LOCOMOTION OF A DROPLET

First, 400 pusher-type squirmers with $\beta = -3.0$ were immersed in the droplet. In this section, the ratio of the droplet radius a^d to the squirmer radius a was set as $a^d/a = 20$, which leads to a volume fraction of 0.05, and Gr was set as $\text{Gr} = 1.0$. We can observe the collective motion of squirmers in the confined boundary (cf. Fig. 2 and Supplemental Movie 1 [25]). In this scenario, pushers near the droplet surface tend to swim along the interface, whereas they swim upwards near the center of the droplet. To illustrate swimmer-induced fluid flow, the time-averaged flow field, both inside and outside of the droplet, are shown in Fig. 2(d). Strong upward flow is generated around the center of the droplet, and a stable convection ring is observed inside the droplet. Swimmer-driven flow is transmitted to the outer fluid via the droplet surface, causing the droplet to migrate upwards (in the positive z direction), even without any external force. The time change in the translational velocity of the droplet in the z direction is shown in Fig. 2(a). We set five initial conditions. The average migration speed approached $U_z^d/U = 0.263$. This result clearly indicates that the collective swimming of enclosed microswimmers propels the droplet. We also investigated the effect of squirmer-squirmer interactions by omitting corresponding terms in Eqs. (10) and (12). In this case, we did not see the collective motion of squirmers and the droplet did not move effectively (data not shown). Which suggests interactions among squirmers play a major role in the emergence of a collective motion of squirmers.

Interestingly, the migration direction of the droplet depends on the swimming mode β . When neutral-type swimmers ($\beta = 0$) were inside, we observed stable convection rings inside the droplet [Fig. 2(e)], and the droplet migrated upwards with a speed of $U_z^d/U = 0.242$ (see Fig. 2(b) and Supplemental Movie 2 [25]). These tendencies are similar to the pushers. However, when strong pullers ($\beta = 3.0$) were inside the droplet, the droplet migrated downwards (in the negative z direction) with a speed of $U_z^d/U = -0.189$ (cf. Fig. 2(c) and Supplemental Movie 3 [25]). In the case of strong pullers, swimmer-driven convections were induced only around the bottom half of the droplet, and the flow direction reversed in the vicinity of the droplet surface [Fig. 2(f)]. By increasing β , the puller-type swimmers tended to become entrapped at the interface due to the hydrodynamic torque [13]. The orientation of pullers was downwards, as shown in Fig. 3(c), which is qualitatively different from that of pushers and neutral-type swimmers [Figs. 3(a) and 3(b)]. The difference in orientation generates a different velocity field external to the droplet, as shown in Fig. 3. In the case of pullers, the external flow is upwards, whereas in the case of pushers, the external flow is downwards. These results suggest that the flow at the interface likely governs the droplet motion. We next investigated the propulsion mechanism with respect to the swimming mode β .

VI. LOCOMOTION MECHANISM

There are two possible locomotion mechanisms: pressure-driven locomotion and surface velocity-driven locomotion. Due to the boundary condition of $\mathbf{q} \cdot \mathbf{t} = 0$, the traction

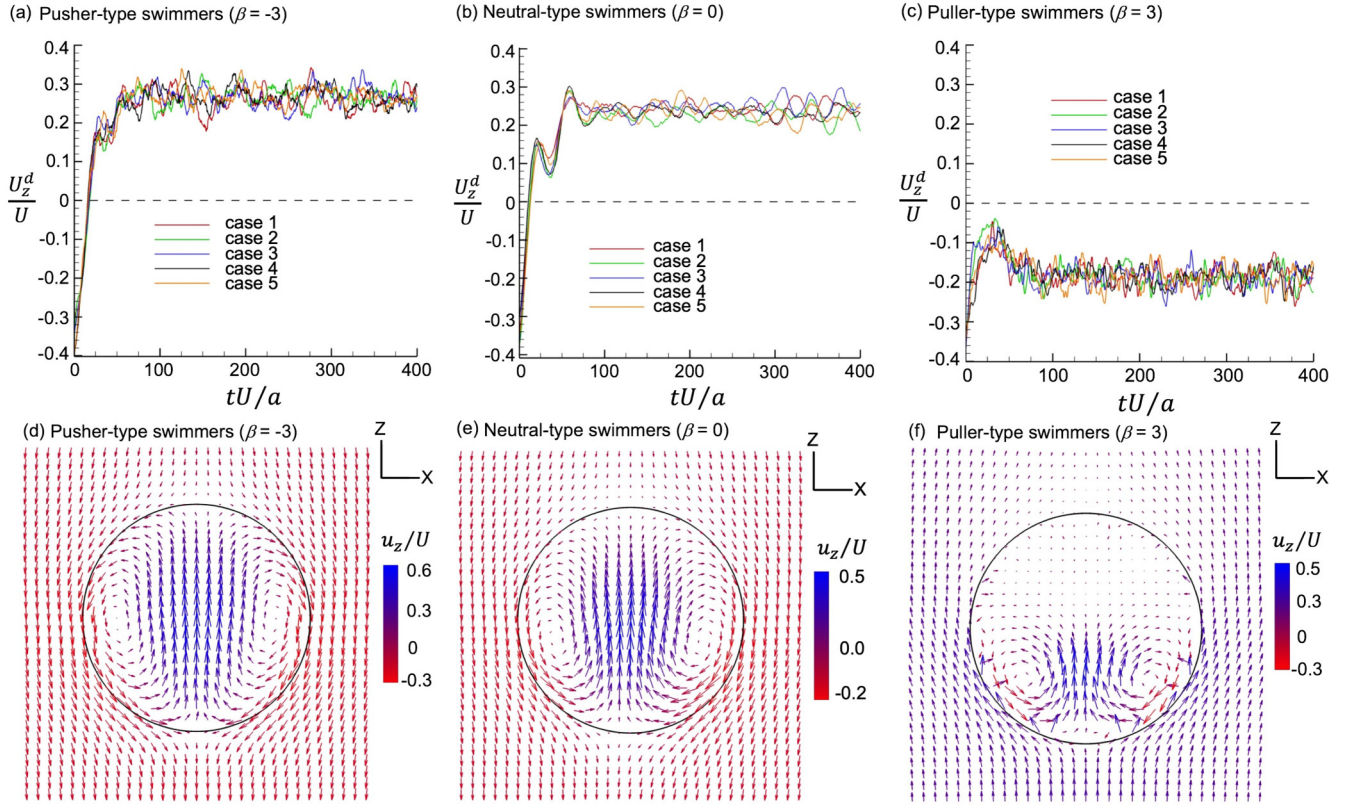


FIG. 2. Migration of the droplet ($Gr = 1.0$, volume fraction = 0.05). (a)–(c) Time change of the vertical locomotion velocity of the droplet containing pushers ($\beta = -3$), neutral ($\beta = 0$), or pullers ($\beta = 3$). We set five different initial conditions in each β . (d)–(f) Time-averaged fluid flow inside and outside of the droplet containing pushers, neutral swimmers, or pullers (with the reference frame of the droplet).

exerted on the droplet surface \mathbf{q} is equivalent to the pressure jump across the interface. The integral of the traction over the surface is zero, i.e., $\int \mathbf{q} dS = 0$, due to the force-free condition of the droplet. Thus, the droplet is not driven by pressure, but by the surface velocity. To confirm this hypothesis, we compared our results with the Lighthill-Blake theory [11,12], in which the locomotion velocity U is correlated with the first-mode squirming velocity B_1 as $U = 2B_1/3$. We define the spherical coordinate (r, θ, ϕ) with the origin at the center of the droplet: r is the radial distance, θ is the elevation angle relative to the swimming direction, and ϕ is the swirl

angle. Time-averaged surface velocities at $r = a$ with pushers ($\beta = -3$), pullers ($\beta = 3$), and neutral squirmers ($\beta = 0$) are shown in Fig. 4 (each data point is taken from the computational node on the droplet surface). The squirming velocity of the squirmer up to the second mode is given by

$$u_\theta = B_1 \sin \theta + B_2 \sin \theta \cos \theta, \quad (23)$$

and then coefficients B_1 and B_2 are determined by the least-squares fitting (green line in Fig. 4). The prediction using the Lighthill-Blake theory shows excellent agreement with the simulation results, regardless of the value of β , as shown in

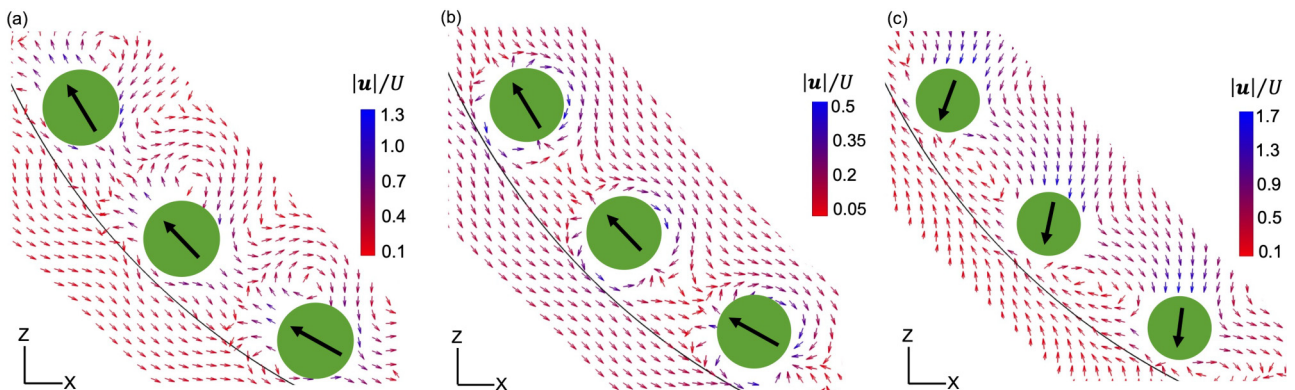


FIG. 3. Fluid flow near the droplet surface created by (a) pushers ($\beta = -3$), (b) neutral swimmers ($\beta = 0$), and (c) pullers ($\beta = 3$) with $Gr = 1.0$ and volume fraction = 0.05. The arrows in squirmers indicate time-averaged orientations of the squirmers near the interface.

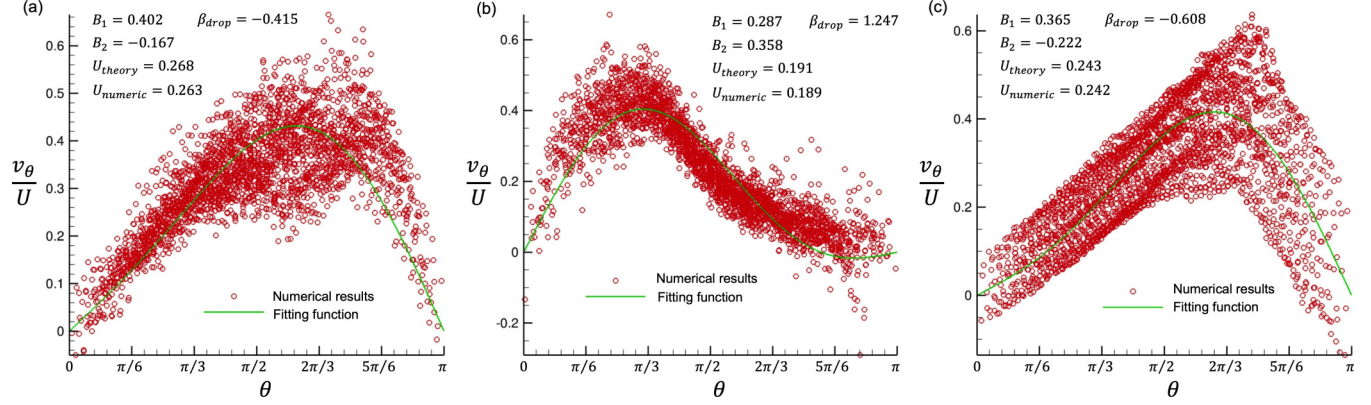


FIG. 4. Time-averaged surface velocity of the droplet with (a) pushers ($\beta = -3$), (b) pullers ($\beta = 3$), and (c) neutral squirmers ($\beta = 0$). The green line indicates least-squares fitting by Lighthill-Blake theory [11]. U_{theory} and β_{drop} are calculated from the fitting results of β_1 and β_2 . U_{numeric} is the numerical result of Fig. 2.

Table I. Thus, we can conclude that the droplet locomotion is driven by the surface velocity, and the locomotion velocity is two-thirds that of B_1 . We also found that, when pushers and neutral squirmers are inside the droplet, the swimming mode of the active droplet is categorized as a pusher [cf. β_{drop} is negative in Figs. 4(a) and 4(c)], while in the case of pullers, the droplet is also categorized as a puller [positive β_{drop} in Fig. 4(b)]. In the study of Reigh *et al.* [10], a single squirmer was immersed in a droplet, which led to the inverted flow field on the surface of the droplet. For example a confined puller created the flow field of a pusher outside the droplet. When a single squirmer was immersed in a droplet, the droplet was migrated by a force dipole exerted on the swimmer body. When the force dipole is negative, i.e., a puller inside, the squirmer pulls the inner fluid and the droplet pushes the outer fluid through the surface flow (vice versa in pushers). In this study, on the other hand, the swimmer-driven flow was driven by the collective motion of squirmers, not by a single force dipole, and the outside flow field corresponded to the swimming mode of the inside swimmers.

VII. EFFECT OF SWIMMING MODE AND VOLUME FRACTION

Next, we seek the optimal parameters for droplet locomotion. The effect of the swimming mode β is shown in Fig. 5(a); the volume fraction was fixed at 0.05 for all cases, and each translational velocity was averaged over five initial conditions. Gr was also fixed to 1.0 in this section. When $\beta \leq 1$, the velocity became positive, and the droplet migrated

upward. The peak value was obtained with weak pushers ($\beta = -1$), and the velocity decreased with β . In the case of strong pushers ($\beta = -2$ and -3), the orientations of the squirmers were disturbed by the strong hydrodynamic interactions among them, which weakened the stable convection ring inside the droplet and eventually reduced the locomotion velocity. However, strong pullers ($\beta \geq 2$) stuck to the surface more strongly as β increased, which increased the surface velocity and the locomotion velocity of the droplet. In the case of weak pullers (e.g., $\beta = 1$), the hydrodynamic torque was relatively weak, and squirmers tended to swim along with the surface. Accordingly, two convection rings could be generated within the droplet, and the droplet migrated upwards similarly to the neutral type. When β is larger than 1, on the other hand, a recirculation region appears in front of a solitary squirmer, and the flow field is qualitatively changed. Moreover, as β increases, the hydrodynamic torque becomes dominant, and squirmers tend to be trapped more frequently at the surface. These differences induced the dynamics change of the droplet movement with β .

We also investigated the effect of volume fraction; the results are shown in Fig. 5(b). When $\beta \leq 0$, the fastest locomotion velocity appeared at the 2.5% volume fraction. A further increase in the volume fraction disturbed the orientations of squirmers, due to the strong hydrodynamic interactions between them, which again weakened the stable convection inside the droplet and eventually decreased the locomotion velocity. In the case of strong pullers ($\beta = 3$), on the other hand, the downward locomotion speed of the droplet increased monotonically with the volume fraction. A droplet containing pullers migrates via the surface velocity generated by stuck particles, as opposed to internal convection. In high volume fraction cases, a large number of pullers stick to the surface, and the swimmer-driven flow and the locomotion velocity increase with the volume fraction. Thus, the effects of the volume fraction differ between pushers and pullers.

TABLE I. Summary of the droplet velocity.

Swimming mode of squirmers	Velocity of the droplet obtained in the simulation	Velocity of the droplet predicted by Ref. [11]
β	U_z^d/U	U_z^d/U
-3.0	0.263	0.268
0.0	0.242	0.243
3.0	-0.189	-0.191

VIII. EFFECTS OF BOTTOM HEAVINESS AND SEDIMENTATION

Next, we ask a simple question: does bottom heaviness or sedimentation play the most crucial role in droplet

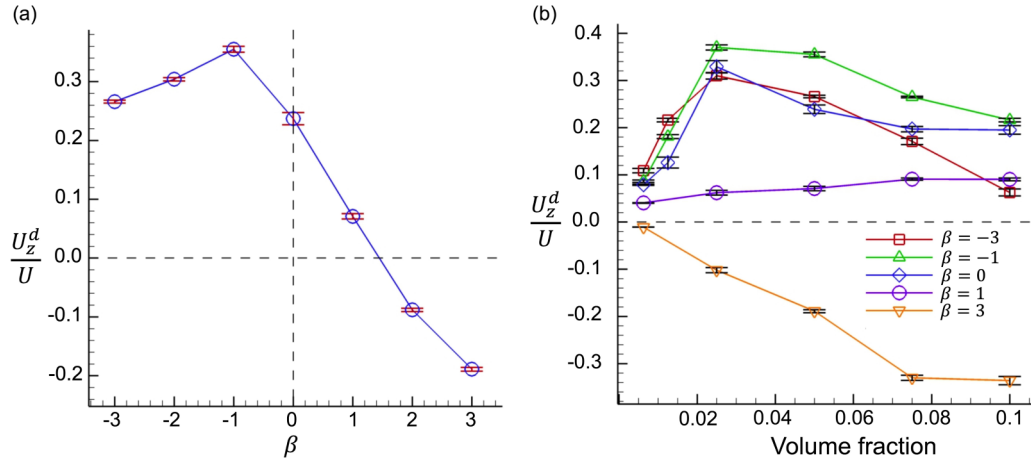


FIG. 5. Effects of parameters on the vertical locomotion velocity. Each plot is averaged by five different initial conditions, and error bars indicate the standard deviation. (a) Effect of swimming mode β (volume fraction = 0.05). (b) Effect of volume fraction of microswimmers.

locomotion? Here, we divided the effects of gravity into sedimentation and bottom heaviness and investigated their contributions to droplet locomotion. The results considering sedimentation only, bottom heaviness only, and their combination (full simulation) are shown in Fig. 6. The results with sedimentation only agree qualitatively with those of the full simulation. The flow field around the droplet is shown in Fig. 6, illustrating that the flow field is also similar to that of the full simulation. When only the effect of bottom heaviness is considered, the droplet always migrates upwards, regardless of β . In this case, almost all squirmers gather at the top of the droplet; notably, the flow field differs considerably from that of the full simulation. If the effect of gravity was turned off, i.e., Gr was set as $Gr = 0$, the flow structure within the droplet was isotropic, and we did not observe effective locomotion of the droplet (see the Appendix). The sedimentation could break the symmetry of the configuration, thus we can

conclude that sedimentation plays the dominant role in droplet locomotion.

IX. EFFECT OF Gr

Last, we investigated droplet locomotion with Gr as a parameter. In Fig. 7, the locomotion velocity and the flow field with various Gr and β are shown. We see the locomotion velocity decreased in both high- and low- Gr regimes. In the high- Gr regime, the sedimentation was dominant and the squirmers accumulated at the bottom of the droplet regardless of the swimming mode β (cf. Supplemental Movie 5 [25]). Accordingly, the swimmer-driven convection was weakened in the high- Gr regime. In the low- Gr regime, on the other hand, pushers and neutral squirmers swam rather randomly and we did not see effective locomotion of the droplet (cf. Supplemental Movie 4 [25]). In the case of pullers with low

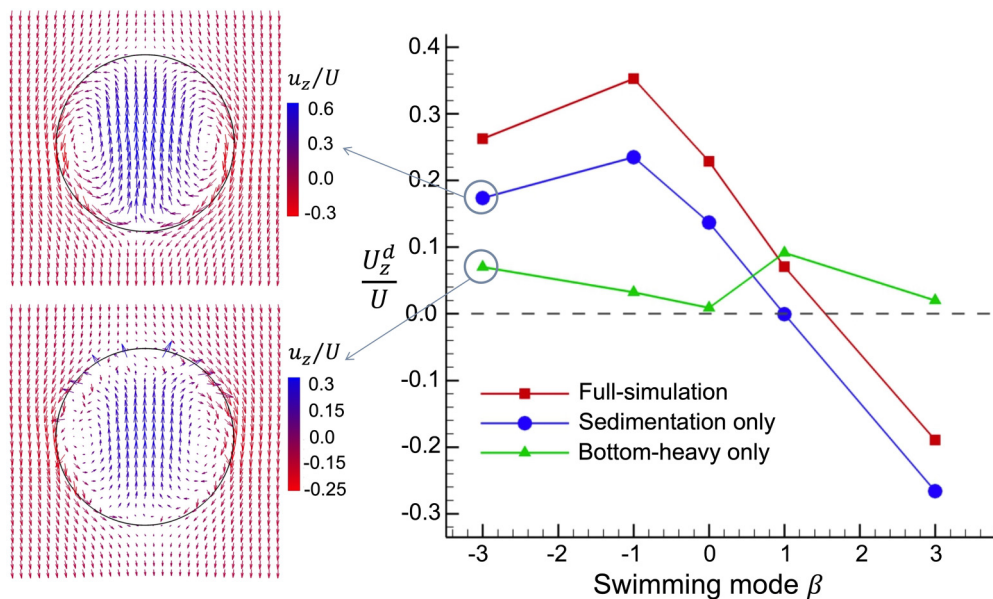


FIG. 6. Vertical locomotion velocity induced by sedimentation only, bottom heaviness only, and both of them (full simulation). The insets show the time-averaged fluid flow generated only by the sedimentation effect or only by the bottom-heavy effect. The volume fraction is 0.05.

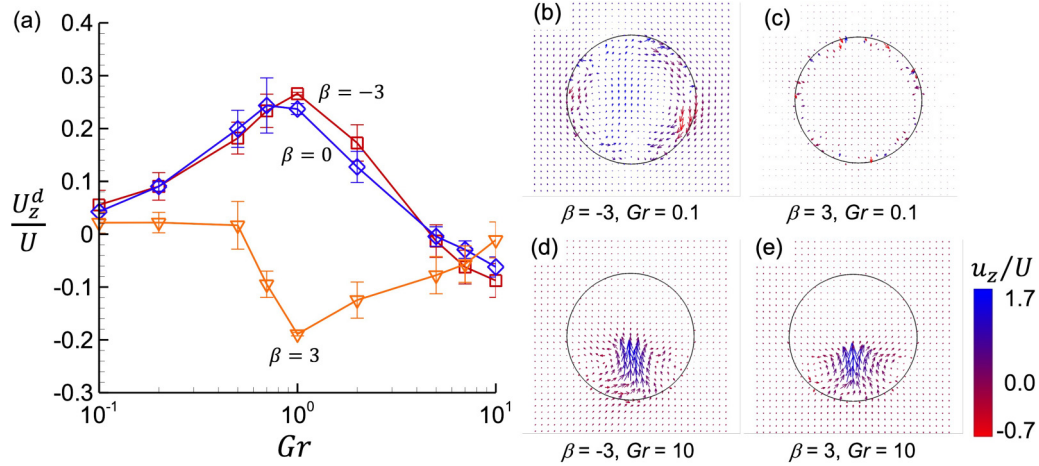


FIG. 7. Effect of the gravity Gr . (a) Locomotion velocity of the droplet as a function of Gr . Each plot is averaged by five different initial conditions, and error bars indicate the standard deviation. (b)–(e) Time-averaged fluid flow inside and outside of the droplets containing pushers or pullers with $Gr = 0.1$ and $Gr = 10$.

Gr , squirmers were tended to be entrapped at the surface, and they oriented toward the outward normal direction as shown

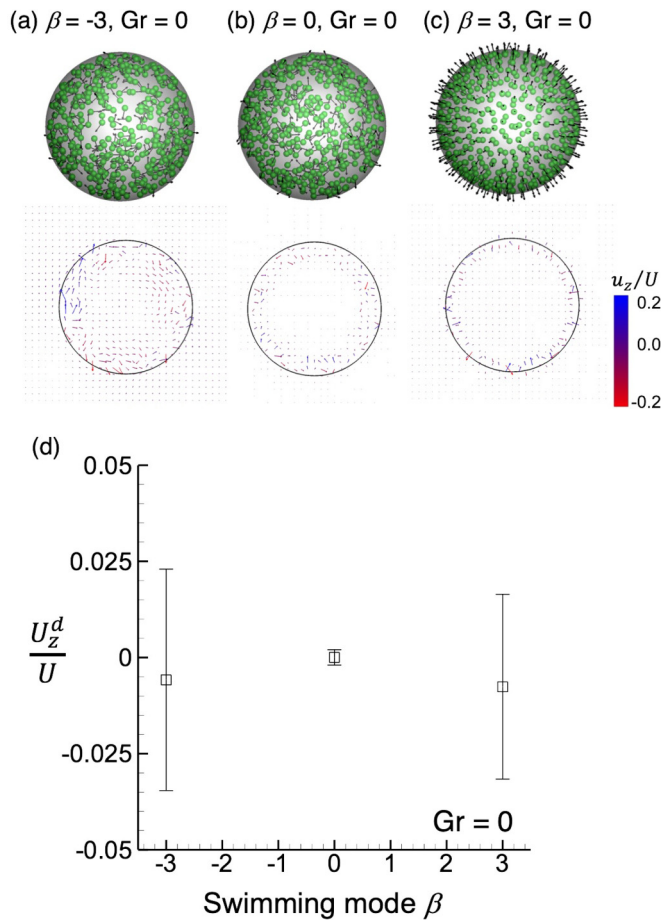


FIG. 8. Droplets containing pusher-, neutral-, or puller-type swimmers with $Gr = 0$. (b), (c) Temporal profiles of the droplet and time-averaged flow field with (a) pushers ($\beta = -3$), (b) neutral-swimmers ($\beta = 0$), and (c) pullers ($\beta = 3$). (d) Locomotion velocity of the droplet as a function of β . Each result is averaged by five initial conditions and error bars indicate the standard deviation.

in Supplemental Movie 8 [25]. Swimmer-driven flow thus became symmetric and we again concluded noneffective locomotion of the droplet with pullers in the low- Gr regime. When the effect of gravity was turned off, i.e., $Gr = 0$, the particle configuration became isotropic and we did not observe droplet migration as shown in Fig. 8.

X. CONCLUSION

In this study, we proposed an active droplet driven by the collective motion of squirmers under gravity. Our results indicate that droplet locomotion can be controlled by changing the swimming mode and the number of microorganisms. The locomotion mechanism of the droplet can be well explained by the Lighthill-Blake theory. In all cases, the locomotion speed of the droplet reaches a maximum when the swimmers inside are weak pushers. These findings are essential to understand the interplay between the motion of suspended self-propelled particles and the bulk motion of active matter, and they pave the way for applications such as manipulation, self-mixing, micropumping, and targeted drug delivery.

ACKNOWLEDGMENTS

The authors acknowledge the funding from the Japan Society for the Promotion of Science (Grants No. 17H00853 and No. 18K18354).

APPENDIX: DROPLET LOCOMOTION UNDER THE $Gr = 0$ CONDITION

In this Appendix, we show the results with $Gr = 0$. The other parameters are the same as those in Fig. 2. In Fig. 8 and Supplemental Movies 6–8 [25], the movement of the droplets containing pushers ($\beta = -3$), neutral swimmers ($\beta = 0$), or pullers ($\beta = 3$) is shown.

In the case of pushers and neutral swimmers, they swam randomly within the droplet, and time-averaged flow was

weakened as shown in Figs. 8(a) and 8(b). Accordingly, we did not observe effective locomotion of the droplet with $\beta = -3$ and 0 [Fig. 8(d)]. In the case of pullers, all squirmers were entrapped at the surface and they oriented toward the

outward normal direction [Fig. 8(c)]. The swimmer-driven flow thus became symmetric, and we again concluded that there was noneffective locomotion of the droplet with pullers ($\beta = 3$).

-
- [1] T. Gao and Z. Li, *Phys. Rev. Lett.* **119**, 108002 (2017).
 - [2] N. Kumar, R. Zhang, J. J. de Pablo, and M. L. Gardel, *Sci. Adv.* **4**, eaat7779 (2018).
 - [3] J. Löber, F. Ziebert, and I. S. Aranson, *Soft Matter* **10**, 1365 (2014).
 - [4] S. Ramaswamy, *Annu. Rev. Condens. Matter Phys.* **1**, 323 (2010).
 - [5] D. Saintillan, *Annu. Rev. Fluid Mech.* **50**, 563 (2018).
 - [6] T. R. Kirkpatrick and J. K. Bhattacherjee, *Phys. Rev. Fluids* **4**, 024306 (2019).
 - [7] A. Loisy, J. Eggers, and T. B. Liverpool, *Phys. Rev. Lett.* **121**, 018001 (2018).
 - [8] E. Lushi, H. Wioland, and R. E. Goldstein, *Proc. Natl. Acad. Sci. USA* **111**, 9733 (2014).
 - [9] A. C. H. Tsang and E. Kanso, *Phys. Rev. E* **91**, 043008 (2015).
 - [10] S. Y. Reigh, L. Zhu, F. Gallaire, and E. Lauga, *Soft Matter* **13**, 3161 (2017).
 - [11] J. Blake, *J. Fluid Mech.* **46**, 199 (1971).
 - [12] M. J. Lighthill, *Commun. Pure Appl. Math.* **5**, 109 (1952).
 - [13] T. Ishikawa, *J. Appl. Phys.* **125**, 200901 (2019).
 - [14] J. Manabe, T. Omori, and T. Ishikawa, *J. Fluid Mech.* **892**, A9 (2020).
 - [15] K. Kyoya, D. Matsunaga, Y. Imai, T. Omori, and T. Ishikawa, *Phys. Rev. E* **92**, 063027 (2015).
 - [16] C. Dombrowski, L. Cisneros, S. Chatkaew, R. E. Goldstein, and J. O. Kessler, *Phys. Rev. Lett.* **93**, 098103 (2004).
 - [17] L. H. Cisneros, J. O. Kessler, S. Ganguly, and R. E. Goldstein, *Phys. Rev. E* **83**, 061907 (2011).
 - [18] A. Sokolov and I. S. Aranson, *Phys. Rev. Lett.* **109**, 248109 (2012).
 - [19] T. Ishikawa, T. J. Pedley, and T. Yamaguchi, *J. Theor. Biol.* **249**, 296 (2007).
 - [20] S. Kim and S. J. Karrila, *Microhydrodynamics: Principles and Selected Applications* (Dover, New York, 1991).
 - [21] T. Omori and T. Ishikawa, *Phys. Rev. E* **93**, 032402 (2016).
 - [22] T. Omori, T. Ishikawa, Y. Imai, and T. Yamaguchi, *J. Biomech.* **46**, 548 (2013).
 - [23] T. Morita, T. Omori, and T. Ishikawa, *Phys. Rev. E* **98**, 023108 (2018).
 - [24] T. Ishikawa, M. P. Simmonds, and T. J. Pedley, *J. Fluid Mech.* **568**, 119 (2006).
 - [25] See Supplemental Material at <http://link.aps.org/supplemental/10.1103/PhysRevE.102.022603> for movies of the droplet locomotion with various swimming modes and gravity forces.